MNRAS **000**, 000–000 (0000) Preprint 8 November 2018 Compiled using MNRAS LATEX style file v3.0

# Near and Mid-infrared properties of known $z \geq 5$ Quasars

Nicholas P. Ross[1⋆] and Nicholas J. G. Cross[1]
[1] *Institute for Astronomy, University of Edinburgh, Royal Observatory, Edinburgh, EH9 3HJ, United Kingdom*

8 November 2018


## ABSTRACT

In this paper, we, for the first time since the discovery of $z \geq 5$ quasars, assemble all spectroscopically confirmed very high redshift quasars in one catalogue. In particular we present the near ($zZyYJHK_s$ and $K$) infrared and mid-infrared (WISE) properties of all 424 spectroscopically confirmed redshift $z \geq 5.00$ quasars. Using archival public WFCAM/UKIRT and VIRCAM/VISTA data we check for photometric variability in the near-infrared that might be expected from Super-Eddington accretion and find *blah*. We present a comprehensive series of colour-redshift and colour-colour plots and make inferences into the hot dust properties of the very high-redshift quasar population. Extrapolating the known quasar luminosity function we suggest that $x$% of the possibly detected $z \geq 5$ quasars in the current datasets have been discovered.


**Key words:** Astronomical data bases: surveys – Quasars: general – galaxies: evolution – galaxies: infrared.

## 1 INTRODUCTION

Very high redshift quasars (VH$z$Q; defined here to have redshifts $z \geq 5.00$) are excellent probes of the early Universe. This includes studies of the Epoch of Reionization for hydrogen (see e.g. Fan et al. 2006; Mortlock 2016, for reviews), the formation and build-up of supermassive black holes (e.g., Rees 1984; Wyithe & Loeb 2003; Volonteri 2010; Agarwal et al. 2016; Valiante et al. 2018; Latif et al. 2018) and early metal enrichment (see e.g., Simcoe et al. 2012; Chen et al. 2017; Bosman et al. 2017).

Super-critical accretion, where $\dot{M} > \dot{M}_{\rm Edd}$, is a viable mechanism to explain the high, potentially super-Eddington, luminosity and rapid growth of supermassive black holes in the early universe (e.g., Alexander & Natarajan 2014; Madau et al. 2014; Volonteri et al. 2015; Pezzulli et al. 2016; Lupi et al. 2016; Pezzulli et al. 2017; Takeo et al. 2018). Thus, one might well expect VH$z$Qs to vary in luminosity as they potentially go through phases of super-critical accretion and these signatures of photometric variability should be looked for, noting the rest-frame optical emission is redshifted into the observed near-infrared (NIR) at redshifts $z > 5$. Fortunately, data are now in place from deep, wide-field NIR instruments and surveys such as the Wide Field Camera (WFCAM) instrument on the United Kingdom Infra-Red Telescope (UKIRT) in the Northern Hemisphere and the VISTA InfraRed CAMera (VIRCAM) on the Visible and Infrared Survey Telescope for Astronomy (VISTA) in the Southern Hemisphere, that are necessary for identifying VH$z$Qs.

Quasars are known to be prodigious emitters of infrared emission, thought to be from the thermal emission of dust grains heated by continuum emission from the accretion disc (e.g., Richards et al. 2006; Leipski et al. 2014; Hill et al. 2014; Hickox et al. 2017). Observations in the mid-infrared, e.g. ∼3-30$\mu$m allow discrimination between AGN[1] and passive galaxies due to the 1.6$\mu$m "bump" entering the MIR at $z \approx 0.8-0.9$ (e.g., Wright et al. 1994; Sawicki 2002; Lacy et al. 2004; Stern et al. 2005; Richards et al. 2006; Timlin et al. 2016) as well as between AGN and star-forming galaxies due to the presence of Polycyclic Aromatic Hydrocarbon (PAHs) at $\lambda > 3\mu$m (e.g., Yan et al. 2007; Tielens 2008).

Jiang et al. (2006) and Jiang et al. (2010) report on the discovery of a quasar without hot-dust emission in a sample of 21 $z \approx 6$ quasars. Such apparently hot-dust-free quasars have no counterparts at low redshift. Moreover, those authors demonstrate that the hot-dust abundance in the 21 quasars builds up in tandem with the growth of the central black hole. But understanding how dust first forms and appears in the central engine remains an open question (Wang et al. 2008, 2011).

WISE mapped the sky in 4 passbands, in bands centered at wavelengths of 3.4, 4.6, 12, and 23$\mu$m. The all

[1] Historically, "quasars" and "Active Galactic Nuclei (AGN)" have described different luminosity/classes of objects, but here we use these terms interchangeably, with a preference for quasar, in recognition of the fact that they both describe accreting supermassive black holes (e.g. Haardt et al. 2016).

⋆ Corresponding Author: npross@roe.ac.uk

sky "ALLWISE" catalog release, contains nearly 750 million detections at high-significance[2], of which over 4.5M AGN candidates have been identified with 90% reliability (Assef et al. 2018). Blain et al. (2013) presented WISE mid-infrared (MIR) detections of 17 (55%) of the then known 31 quasars at $z > 6$. However, Blain et al. (2013) was compiled with the WISE 'All-Sky' data release, as opposed to the superior "AllWISE" catalogs. That sample only examined the 31 known $z > 6$ quasars; our sample has 148 (**NPR to Double Check!**) objects with redshift $z \geq 6.00$.

Critically, we now have available to us new W1 and W2 photometry from the 'unWISE Source Catalog' (Schlafly & Meisner 2018), a WISE-selected catalog that is based on significantly deeper imaging and has a more extensive modeling of crowded regions than the ALLWISE release. For the first time in a catalog, unWISE takes advantage of the ongoing mid-IR Near-Earth Object Wide-Field Infrared Survey Explorer Reactivation mission (NEOWISE-R; Mainzer et al. 2014), and achieves depths ∼0.7 mag deeper than ALLWISE (in W1/2). This additional depth is a significant advantage in the detection and study of VH$z$Qs in the 3-5 micron regime.

Here we update Jiang et al. (2010) and Blain et al. (2013) (along with Table 8 of Bañados et al. 2016). Our motivations are numerous and include: *(i)* establishing the first complete catalogue of $z > 5.00$ quasars since the pioneering work from SDSS; *(ii)* analyzing all the WFCAM and VISTA near-infrared photometry for the quasars; *(iii)* making the first study of NIR variability of the VHzQ population and *(iv)* establishing the photometric properties for upcoming surveys and telescopes, e.g. the Large Synoptic Survey Telescope (LSST)[3], ESA *Euclid*[4] and the *James Webb Space Telescope* (JWST)[5,6,7,8].

This paper can be considered an update of Blain et al. (2013) and also an extension of parts of Bañados et al. (2016), with the latter study reporting WISE W1, W2, W3 and W4 magnitudes for the Panoramic Survey Telescope and Rapid Response System 1 (Pan-STARRS1, PS1; Kaiser et al. 2002, 2010), but with no further investigation into the reddest WISE waveband for the VH$z$Qs. Bañados et al. (2016) reports and investigates the W1, W2 and W3 properties of quasars at $z > 5.6$. We chose redshift $z = 5.00$ as our lower redshift limit due to a combination of garnishing a large sample, adequately spanning physical properties (e.g. luminosity, age of the Universe) and to incorporate what knowledge we have gained over the last couple of decades since $z > 5$ quasars were discovered.

This paper is organized as follows. In Section 2, we present the assembled list of the 424 $z \geq 5.00$ VH$z$Qs that we have compiled. We then give a high-level overview of the photometric surveys and datasets we use and present the photometry of the VH$z$Qs. In Section 3 we ... and In Section 4 we ... We conclude in Section 5 and present all the necessary details to obtain our dataset in the Appendices.

[2] wise2.ipac.caltech.edu/docs/release/allwise/expsup/sec2_1.html
[3] lsst.org
[4] sci.esa.int/euclid/
[5] jwst.nasa.gov;
[6] sci.esa.int/jwst;
[7] www.asc-csa.gc.ca/eng/satellites/jwst;
[8] jwst.stsci.edu

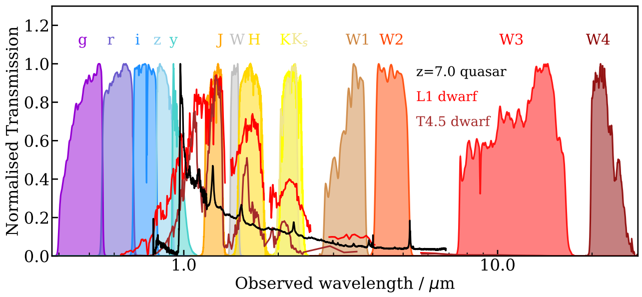


**Figure 1.** The spectral bands used by different survey telescopes and that are relevant here. The *grizy* filters are from the Pan-STARRS survey. The $JHK$ are from UKIRT/WFCAM, while $K_s$ is a VISTA/VIRCAM filter. The The narrow W-band centered at $\lambda \approx 14,500$Å is a CFHT/Wircam filter. [NJC: Do we use the W-band anywhere?] The WISE passbands W1-4 are also presented. The quasar spectrum is a composite based on Vanden Berk et al. (2001) and Bañados et al. (2016). The L and T dwarf spectra are from Cushing et al. (2006).

We make the decision to present all our photometry and magnitudes on the AB zero-point system (Oke & Gunn 1983; Fukugita et al. 1996). This includes the near-infrared, as well as the mid-infrared magnitudes. Appendix **??** gives the AB to Vega transforms for a wide range of optical, NIR and MIR filters. We use a flat ΛCDM cosmology with $H0 = 67.7$ km s−1 Mpc1, $\Omega_{\rm M} = 0.307$, and $\Omega_\Lambda = 0.693$ (Planck Collaboration et al. 2016) in order to be consistent with Bañados et al. (2016).

## 2 DATA

In Table 1 we present our dataset and we have assembled this in the following manner. First we compile the list of all known, spectroscopically confirmed quasars from the literature. Most of these objects are easily identified by their broad Ly$\alpha$ emission line, N V emission and characteristic shape blueward of 1215Å in the rest-frame. As we shall see, some of the more recently discovered objects are close to the galaxy luminosity function characteristic luminosity $M^*$, and some have relatively weak or maybe even completely absorbed Ly$\alpha$ (e.g. Figures 7 and 10 in Bañados et al. 2016). We leave aside detailed investigation and discussion into spectral features and line strengths, and take as given the published spectra and identifications.

We then obtain optical, near-infrared and mid-infrared photometry for the spectral dataset. The optical data comes from the Panoramic Survey Telescope and Rapid Response System (Pan-STARRS) survey (Chambers et al. 2016). The near-infrared data comes from two sources: first, the WFCAM (Casali et al. 2007) on the UKIRT, primarly, but not exclusively, as part of the UKIRT Infrared Deep Sky Survey (UKIDSS; Lawrence et al. 2007). And second, data from the VIRCAM on the VISTA (Emerson et al. 2006; Dalton et al. 2006). The mid-infrared, $\lambda = 3 - 30\mu$m wavelength data is from the the Wide-Field Infrared Survey Explorer (WISE; Wright et al. 2010; Cutri 2013) mission.

For reference, Figure 1 displays the wavelength and normalised transmission of the filters in question.

| na | desig | ra_hms | dec_dms | ra | dec | redshift | mag | M1450 | ref |
|---|---|---|---|---|---|---|---|---|---|
| PSO | J000.3401+26.8358 | 00:01:21.63 | +26:50:09.17 | 0.340113 | +26.83588 | 5.75 | 19.52 | -27.16 | 1/1/1 |
| SDSS | J0002+2550 | 00:02:39.39 | +25:50:34.80 | 0.664117 | +25.84304 | 5.82 | 19.39 | -27.31 | 5/22/1 |
| SDSS | J0005-0006 | 00:05:52.34 | -00:06:55.80 | 1.468083 | -00.11549 | 5.85 | 20.98 | -25.73 | 5/12/1 |
| PSO | J002.1073-06.4345 | 00:08:25.77 | -06:26:04.60 | 2.107390 | -06.43456 | 5.93 | 20.41 | -26.32 | 1;43/1/1 |
| SDWISE | J0008+3616 | 00:08:51.43 | +36:16:13.49 | 2.214292 | +36.27041 | 5.17 | 19.12 | -27.34 | Wang2016 |
| PSO | J002.3786+32.8702 | 00:09:30.89 | +32:52:12.94 | 2.378702 | +32.87026 | 6.1 | 21.13 | -25.65 | 1/1/1 |
| SDSS | J0017-1000 | 00:17:14.68 | -10:00:55.4 | 4.311166 | -10.01540 | 5.011 | 99.99 | -99.99 | DR7_W16 |
| PSO | J004.3936+17.0862 | 00:17:34.47 | +17:05:10.70 | 4.393614 | +17.08631 | 5.8 | 20.69 | -26.01 | 1/1/1 |
| PSO | J004.8140-24.2991 | 00:19:15.38 | -24:17:56.98 | 4.814080 | -24.29920 | 5.68 | 19.43 | -27.24 | 1/1/1 |
| VDES | J0020-3653 | 00:20:31.46 | -36:53:41.8 | 5.131124 | -36.89495 | 6.9 | 99.99 | -99.99 | DES-VHS_inprep |

**Table 1.** All 424 $z \geq 5.00$ quasars that have been spectroscopically confirmed as of 2018 June. The first ten objects are given here as guidance to the format of the data table. The full table can be found online.

| na | desig | ra | dec | w1mag | w1err | w1snr | w2mag | w2err | w2snr | w3mag | w3err | w3snr | w4mag | w4err | w4snr |
|---|---|---|---|---|---|---|---|---|---|---|---|---|---|---|---|
| PSO | J000.3401+26.8358 | 0.34011348 | 26.83588138 | 16.373 | 0.066 | 16.5 | 15.266 | 0.107 | 10.2 | 12.594 | 0.492 | 2.2 | 8.756 | -9.99 | 1.1 |
| SDSS | J0002+2550 | 0.66411726 | 25.84304425 | 16.162 | 0.057 | 19.0 | 15.542 | 0.127 | 8.5 | 12.416 | 0.423 | 2.6 | 8.683 | -9.99 | 1.2 |
| SDSS | J0005-0006 | 1.4680833 | -0.1154999 | 17.299 | 0.16 | 6.8 | 17.043 | -9.99 | 0.2 | 12.445 | -9.99 | -1.1 | 9.008 | -9.99 | -0.3 |
| PSO | J002.1073-06.4345 | 2.10739 | -6.43456 | 16.809 | 0.107 | 10.1 | 15.684 | 0.141 | 7.7 | 11.892 | -9.99 | 1.5 | 8.759 | -9.99 | 0.2 |
| SDWISE | J0008+3616 | 2.2142917 | 36.2704138 | 16.045 | 0.052 | 20.7 | 15.373 | 0.092 | 11.8 | 12.043 | -9.99 | 1.8 | 8.786 | -9.99 | 1.1 |
| PSO | J002.3786+32.8702 | 2.37870183 | 32.87026179 | -99.99 | -9.99 | -9.9 | -99.99 | -9.99 | -9.9 | -99.99 | -9.99 | -9.9 | -9.99 | -9.99 | -9.9 |
| SDSS | J0017-1000 | 4.3111666 | -10.01539722 | 15.936 | 0.055 | 19.7 | 15.167 | 0.094 | 11.5 | 12.026 | 0.334 | 3.2 | 8.52 | -9.99 | 1.2 |
| PSO | J004.3936+17.0862 | 4.39361347 | 17.08630447 | -99.99 | -9.99 | -9.9 | -99.99 | -9.99 | -9.9 | -99.99 | -9.99 | -9.9 | -9.99 | -9.99 | -9.9 |
| PSO | J004.8140-24.2991 | 4.81408 | -24.29916 | 16.281 | 0.069 | 15.8 | 15.569 | 0.116 | 9.4 | 12.123 | 0.344 | 3.2 | 8.82 | -9.99 | 0.5 |
| VDES | J0020-3653 | 5.1311237 | -36.8949476 | 16.844 | 0.094 | 11.6 | 16.354 | 0.204 | 5.3 | 12.679 | -9.99 | -0.1 | 8.342 | -9.99 | 0.8 |

**Table 2.** The mid-infrared photometric properties from the WISE ALLWISE catalogue for the 424 very-high redshift quasars. The first ten objects are given here as guidance to the format of the data table. The full table can be found online. *This is the third table here; the SECOND table is this with the NIR data...*

| na | desig | ra | dec | w1mag | w1err | w1snr | w2mag | w2err | w2snr | w3mag | w3err | w3snr | w4mag | w4err | w4snr |
|---|---|---|---|---|---|---|---|---|---|---|---|---|---|---|---|
| PSO | J000.3401+26.8358 | 0.34011348 | 26.83588138 | 16.373 | 0.066 | 16.5 | 15.266 | 0.107 | 10.2 | 12.594 | 0.492 | 2.2 | 8.756 | -9.99 | 1.1 |
| SDSS | J0002+2550 | 0.66411726 | 25.84304425 | 16.162 | 0.057 | 19.0 | 15.542 | 0.127 | 8.5 | 12.416 | 0.423 | 2.6 | 8.683 | -9.99 | 1.2 |
| SDSS | J0005-0006 | 1.4680833 | -0.1154999 | 17.299 | 0.16 | 6.8 | 17.043 | -9.99 | 0.2 | 12.445 | -9.99 | -1.1 | 9.008 | -9.99 | -0.3 |
| PSO | J002.1073-06.4345 | 2.10739 | -6.43456 | 16.809 | 0.107 | 10.1 | 15.684 | 0.141 | 7.7 | 11.892 | -9.99 | 1.5 | 8.759 | -9.99 | 0.2 |
| SDWISE | J0008+3616 | 2.2142917 | 36.2704138 | 16.045 | 0.052 | 20.7 | 15.373 | 0.092 | 11.8 | 12.043 | -9.99 | 1.8 | 8.786 | -9.99 | 1.1 |
| PSO | J002.3786+32.8702 | 2.37870183 | 32.87026179 | -99.99 | -9.99 | -9.9 | -99.99 | -9.99 | -9.9 | -99.99 | -9.99 | -9.9 | -9.99 | -9.99 | -9.9 |
| SDSS | J0017-1000 | 4.3111666 | -10.01539722 | 15.936 | 0.055 | 19.7 | 15.167 | 0.094 | 11.5 | 12.026 | 0.334 | 3.2 | 8.52 | -9.99 | 1.2 |
| PSO | J004.3936+17.0862 | 4.39361347 | 17.08630447 | -99.99 | -9.99 | -9.9 | -99.99 | -9.99 | -9.9 | -99.99 | -9.99 | -9.9 | -9.99 | -9.99 | -9.9 |
| PSO | J004.8140-24.2991 | 4.81408 | -24.29916 | 16.281 | 0.069 | 15.8 | 15.569 | 0.116 | 9.4 | 12.123 | 0.344 | 3.2 | 8.82 | -9.99 | 0.5 |
| VDES | J0020-3653 | 5.1311237 | -36.8949476 | 16.844 | 0.094 | 11.6 | 16.354 | 0.204 | 5.3 | 12.679 | -9.99 | -0.1 | 8.342 | -9.99 | 0.8 |

**Table 3.** The mid-infrared photometric properties from the WISE ALLWISE catalogue for the 424 very-high redshift quasars. The first ten objects are given here as guidance to the format of the data table. The full table can be found online. *This is the third table here; the SECOND table is this with the NIR data...*

| Survey | # VHzQs | Notes/Survey reference |
|---|---|---|
| ATLAS | 4 | Shanks et al. (2015) |
| CFHQS | 20 | Willott et al. (2007) |
| DELS | 2 | Dey et al. (2018) |
| ELAIS | 1 | Väisänen et al. (2000) |
| FIRST | 1 | Becker et al. (1995) |
| IMS | 1 | Kim et al. (2015) |
| MMT | 12 | McGreer et al. (2013) |
| NDWFS | 1 | Jannuzi & Dey (1999) |
| PSO | 84 | Kaiser et al. (2002, 2010) |
| RD | 1 | Mahabal et al. (2005) |
| SDSS | 156 | Stoughton et al. (2002) |
| SDUV[a] | 20 | ? |
| SDWISE[b] | 27 | Wang et al. (2016) |
| SHELLQs | [c]63 | Matsuoka et al. (2016) |
| ULAS | 10 | Lawrence et al. (2007) |
| VDES | 11 | Reed et al. (2017) |
| VIK | 9 | Edge et al. (2013) |
| VIMOS | 1 | Le Fèvre et al. (2003) |

**Table 4.** The number of VH$z$Q from given surveys, with the key survey or telescope reference. [a]SDUV = SDSS+ULAS+VHS; [b]SDWISE = SDSS+WISE; [c]Includes 8 objects with a HyperSuprimeCam (HSC; Miyazaki et al. 2018) designation.

### 2.1 Spectroscopy

We have obtained a list of 424 spectroscopically confirmed quasars with redshifts $z \geq 5.00$.

In Table 1 we give the discovery reference for the VH$z$Qs noting that some objects were discovered independently and contemporaneously. The redshifts for the VH$z$Qs generally come from the measurement of broad UV/optical emission lines. Where there are far infra-red emission lines e.g. C II 158 micron, we report these, but at the level of our current analysis broadline redshifts are sufficient.

Specifically, we use data from: Bañados et al. (2014, 2016, 2018), Becker et al. (2015), Calura et al. (2014), Carilli et al. (2007, 2010), Carnall et al. (2015), Cool et al. (2006), De Rosa et al. (2011), Fan et al. (2000, 2001, 2003, 2004, 2006); **?**, Goto (2006), Ikeda et al. (2017), Jiang et al. (2008, 2009, 2015), Kashikawa et al. (2015), Koptelova et al. (2017), Kim et al. (2015), Kurk et al. (2007, 2009), Leipski et al. (2014), Mahabal et al. (2005), Matsuoka et al. (2016, 2018a,b), Mazzucchelli et al. (2017), Morganson et al. (2012), Mortlock et al. (2009, 2011), McGreer et al. (2006, 2013), Reed et al. (2015, 2017), Stern et al. (2007), Tang et al. (2017), Venemans et al. (2007, 2012, 2013, 2015b,a, 2016), Wang et al. (2016, 2017); **?**); **?**, Willott et al. (2007, 2009, 2010,?, 2013, 2015), Wu et al. (2015) **?** and Zeimann et al. (2011),

Table 1 gives the salient details for the objects used in this study. We use all the $z \geq 5.00$ quasars that have been discovered and spectroscopically confirmed as of the time of writing (2018 November). We report near-infrared ($yYJHK$-bands) and mid-infrared (WISE W1/2/3/4) photometry.

### 2.2 Optical Photometry

We query the Panoramic Survey Telescope and Rapid Response System (Pan-STARRS)[9] Data Release 1 (DR1) Catalog Archive Server Jobs System (CasJobs) service at mastweb.stsci.edu/ps1casjobs/. The Pan-STARRS1 (PS1) survey observed the 30,000 deg$^2$ of sky north of declination $-30$ degrees in five filters *grizy*. PS1 is the first part of Pan-STARRS to be completed and is the basis for the DR1. Chambers et al. (2016), Magnier et al. (2016c), Waters et al. (2016), Magnier et al. (2016a), Magnier et al. (2016b) and Flewelling et al. (2016) describe the instrument, survey, and data analyses. The principal science product of the PS1 survey is the catalog accessible through the CasJobs interface.

We query and return the mean PSF magnitudes from the *grizy* filters (`MeanPSFMag`) which are in the AB system for our 424 VH$z$Q sample. Details of our SQL and links to the main tables are given in Appendix **??**.

### 2.3 Near-infrared photometry

The near-infrared data in this paper comes from the Wide Field Astronomy Unit's (WFAU) Science Archives for UKIRT-WFCAM, the WFCAM Science Archive (WSA Hambly et al. 2008) and VISTA-VIRCAM, the VISTA Science Archive (VSA Cross et al. 2012). These archives were developed for the VISTA Data Flow System (VDFS Emerson et al. 2004).

We access both the WSA and the VSA and include all non-proprietary WFCAM data, which covers all public surveys and PI projects from Semester 05A to 1st January 2017, and all non-proprietary VISTA data, which covers all public surveys and PI projects from science verification (20091015) to 1st April 2016.

The data was processed using a matched-aperture photometry method where flux is measured at the spectroscopic position of the quasar, without necessarily knowing if there is a formal detection in the NIR photometry beforehand. Full details of the matched-aperture pipeline will appear in a forthcoming paper, Cross et al. 2018, in prep, and has also been discussed in Cross et al. (2013).

We query the WSA and VSA performing matched-aperature photometry at the positions of our 424 VH$z$Qs. This database is world-readable and we give the full receipe and relevant SQL queries for accessing both databases in Appendix **??**.

#### 2.3.1 *Averaging matched photometry*

The photometry in a single epoch image often has low signal-to-noise. The advantage of matched aperture photometry on QSOs is that co-adding is relatively simple if each epoch is taken in the same aperture and the aperture photometry has been corrected to total. Indeed, the standard aperture corrections work well for point sources. Coadding using the matched-aperature photometry, where the individual epochs are taken from multiple projects with different pointings and orientations, should help with issues such as scattered light, pixel distortion and aperture corrections.

[9] https://outerspace.stsci.edu/display/PANSTARRS

We average the aperture corrected calibrated fluxes (e.g. **aperJky3**), and then convert to magnitudes. Since we do not have a deep image for each set of averages, we cannot calculate non-aperture corrected values, so the photometry is only appropriate for point-sources.

$$\bar{F} = \frac{\sum_i^N (w_i\, F_i)}{\sum_i^N w_i} \tag{1}$$

where $F_i$ is the $i^{th}$ epoch measurement of a parameter to be averaged such as the aperture corrected calibrated flux in a $1''$ aperture (**aperJky3**) and $\bar{F}$ is the weighted mean average of this parameter. The weight for each epoch $w_i = 1/(\sigma_F)^2$ if the epoch is included and $w_i = 0$ if an epoch is excluded for quality control purposes.

We calculate a set of averaged catalogues, for each pointing and filter, based on the requirements in `RequiredMapAverages`, in these cases over time spans of 7, 14, 30, 91, 183 days, 365 days, 730 days, over 10 epochs and over all epochs. **NJC: Should we add this table to suplemental online only material?** The averaging process starts at the first epoch and works on.

We detect 304 unique quasars in the WFCAM WSA database, 203 quasars are detected in the VISTA VSA database with 114 objects in common with both WFCAM and VISTA data. We give the necessary SQL queries syntax in Appendix **??**.

### 2.4 MIR data

The MIR data for this study comes exclusively from the Wide-field Infrared Survey Explorer (WISE) mission. Since we are only concerned here with the very large area ($\gg 1000$ deg$^2$) surveys, we leave exploration of the VH$z$Q population in e.g. the large Spitzer areal surveys such as the Spitzer IRAC Equatorial Survey (SpIES; Timlin et al. 2016), the Spitzer-HETDEX Exploratory Large-area Survey (SHELA; Papovich et al. 2016) and the Spitzer-SPT Deep Field (SSDF; Ashby et al. 2013), to a future investigation. This will also include a detailed study of MIR spectra e.g. Lambrides et al. (2018).

We use data from the the beginning of the WISE mission (2010 January; Wright et al. 2010) through the fourth-year of NEOWISE-R operations (Mainzer et al. 2011, 2017 December;). More specifically, we use the data from the AllWISE program and catalogue, which combines data from the WISE cryogenic and NEOWISE (Mainzer et al. 2011 ApJ, 731, 53) post-cryogenic survey phases. For the our variability investigations, we supplement the ALLWISE data with data from the NEOWISE 2018 Data Release. NEOWISE 2018 makes available the 3.4 and 4.6 m (W1 and W2) single-exposure images and extracted source information that were acquired between 2016 December 13 and 2017 December 13 UTC, which was the fourth year of survey operations of the Near-Earth Object Wide-field Infrared Survey Explorer Reactivation Mission (NEOWISE; Mainzer et al. 2014, ApJ, 792, 30). The fourth year NEOWISE data products are concatenated with those from the first three years (originally released on March 26, 2015, March 23, 2016 and June 1, 2017) into a single archive.

The WISE scan pattern leads to coverage of the full-sky approximately once every six months (a "sky pass"), but the satellite was placed in hibernation in 2011 February and then reactivated in 2013 October. Hence, our light curves have a cadence of 6 months with a 32 month sampling gap.

| Selection | number detected (%) |
|---|---|
| Any band ($ZYJHK/K_s$ | 394 (92.9) |
| $Z$-band | 72 (17.0) |
| $Y$-band | 249 (58.7) |
| $J$-band | 391 (92.2) |
| $H$-band | 258 (60.8) |
| $K$ or $Ks$-band | 297 ( ) |

**Table 5.** Detection rate of VH$z$Qs in the near-infrared.

## 3 RESULTS

Having collated the sample of 424 VH$z$Qs, and obtained their optical, near- and mid-infrared photometry we report here the various photometric properites of the quasars.

First, we will concentrate on detection rate in the infrared, go on to report on the color-redshift and color-color properties of our sample and then report on how the current sample populates the luminosity-redshift $Lz$-plane.

### 3.1 Detection Rates in the NIR

Table 5 gives the detection rates for the VH$z$Qs in the NIR $YJHK/K_s$-bands. The first thing to note is that the coverage of the NIR surveys for example from the UKIDSS LAS and VISTA VHS, does not overlap the full area for where the VH$z$Qs are detected.

#### *3.1.1 Comparing WFCAM and VISTA*

There are 114 overlapping QSOs between WFCAM and VISTA. Using the `VegaToAB` value[10] to put these objects on the same AB system, and for each object compared the two measurements. First, the calculated weighted average (calibrated flux) in each filter of both and calculated the ratio and difference between each measurement and the average. Then for each filter we calculated the weighted average of the differences (in mag) for each instrument to see if there were significant offsets. The results are given in Table 6. The only filter with a significant offset is the $Y$-band. All of the VISTA averages are negative and all of the WFCAM ones are positive. The $Ks$ versus $K$ band may be slightly dodgy, given the different shapes of the filters.

### 3.2 Detection Rates in the MIR

Unlike the NIR coverage, the WISE satellite and mission performed an all-sky survey, so the location of evey VH$z$Q in our dataset is covered. However, the depth of the WISE ALLWISE survey depends heavily on sky location, with locations near the Ecliptic Poles having the highest number of exposures.

[10] What is this exactly??

| abs(VIRCAM - WFCAM) | millimags | no. of objects |
|---|---|---|
| $Z$ | 19.3 | 2 |
| $Y$ | 66.2 | 48 |
| $J$ | 3.2 | 105 |
| $H$ | 19.3 | 89 |
| $K_s/K$ | 12.7 | 93 |

**Table 6.** Comparing the magnitudes in different WFCAM/UKIRT and VIRCAM/VISTA near-infrared bands.

| Selection | number detected (%) |
|---|---|
| W1 SNR > 2.0 | 275 (64.9) |
| W2 SNR > 2.0 | 255 (60.1) |
| W1 ∧ W2 SNR > 2.0 | |
| W3 SNR > 2.0 | 99 (23.3) |
| W4 SNR > 2.0 | 29 (6.8) |
| Any W1/2/3/4 SNR > 2.0 | |
| W1/2 SNR < 2.0 ∧ W3 SNR > 2.0 | |

**Table 7.** ATLAS Shanks et al. (2015);

| Selection | number detected (% of full specrta) |
|---|---|
| From "Source", "Rejects", | 245, 40 (67.2) |
| W1 SNR > 2.0 | 279 (65.8) |
| W2 SNR > 2.0 | 258 (60.8) |
| W1 ∧ W2 SNR > 2.0 | 253 (59.7) |
| W3 SNR > 2.0 | 97 (22.9) |
| W4 SNR > 2.0 | 33 (7.8) |
| W1/2 SNR < 2.0 ∧ W3 SNR > 2.0 | 3 (0.7) |

**Table 8.** Data from the AllWISE Source Catalog and AllWISE Reject Table, from the `NASA/IPAC Infrared Science Archive`

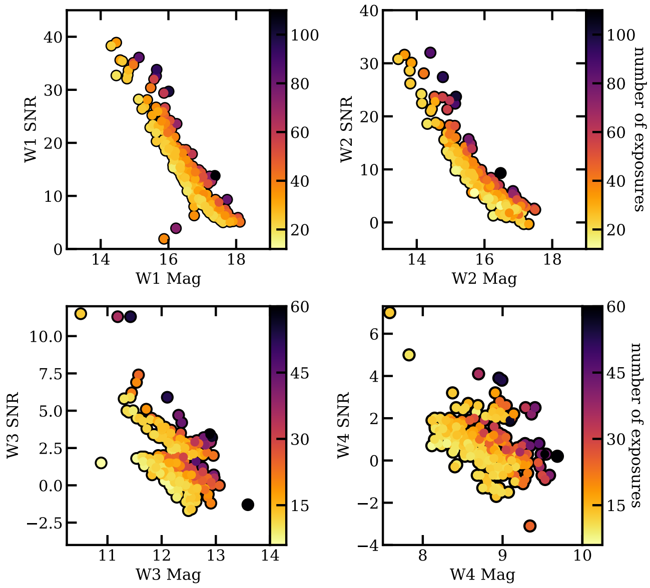


**Figure 2.** WISE W1/2/3/4 magnitude against signal-to-noise, colour coded by w$x$cov the mean coverage depth, in each corresponding band.

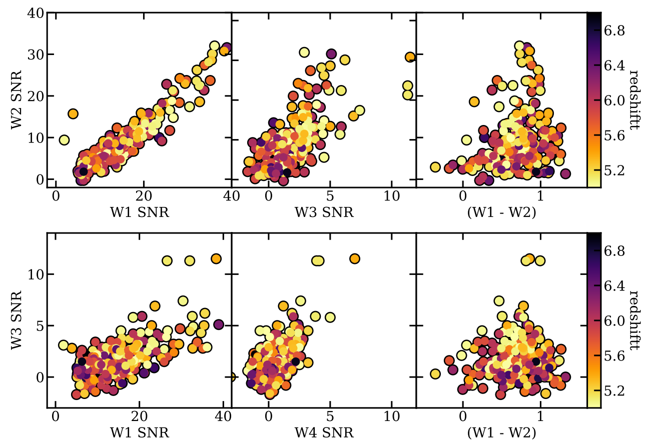


**Figure 3.** WISE signal-to-noise measures for the four bands, as well as for (W1-W2) colour. The points are colour coded by redshift.

Before reporting on the detection rates, we investigate this effect. Figure 3 shows the WISE magnitude versus signal-to-noise, colour coded by `w`$x$`cov` the mean coverage depth, in each corresponding band. In the two shorter bands W1/2 we see the clear and expected trend for brighter objects to have larger SNR, and also for the higher signal to noise for objects with more exposures at a given magnitude. The behaviour for the W3/4 bands is different, with two populations clearly evident in W3 and although a bit more mixed, also in W4. With the suggested split at SNR> 2, and no obvious R.A./Declination dependence seen, this behaviour is explained by the fact that there are non-detectiopns in W3/4 for objects (with high W1/2 SNR) that are reported in the ALLWISE catalogue.

For the 278 VH$z$Q with coverage detections, the mean number of exposures for the W1/2 bands is 32.0 and 31.5, respectively, with a minimum number of exposures 17 and 12, and the maximum number or exposures being 114 (for both bands). For the W3/4 filters, the corresponding mean, minimum and maximum exposure are 17.4 and 17.5, 5.8 and 6.8 and 69 (for both bands). These values are direclty from the `w`$x$`cov` enteries in the WISE ALLWISE catalogue.

Table 8 gives the detection rates for the VH$z$Qs in the MIR WISE W1-4 bands.

Blain et al. (2013)

Recently, Assef et al. (2018) released two large catalogues of AGN candidates identified across 30,000 deg$^2$ of extragalactic sky from the WISE AllWISE Data Release. The "R90" catalogue, is contains 4.5M AGN candidates at 90% reliability (and ≈150 AGN candidates per deg$^2$) while the "C75" catalog consists of 20.9M AGN candidates at 75% completeness (and (≈700 AGN candidates per deg$^2$). Cross-matching out catalogue of 424 VH$z$Qs with these catalogues, produces 42 matches with the R90 sample and 98 matches with the C75 sample. Both catalogues unsurprisingly match to the ultraluminous quasar SDSS J0100+2802 (Wu et al. 2015) while the C75, but not the R90 catalogue mathes to ULAS J1120+0641 (Mortlock et al. 2011). Neither catalogue matches J1342+0928 (Bañados et al. 2018).

Very High-$z$ Quasars Detected in WISE W3 and W4.

### 3.3 Variability

VH$z$Qs, if accreting at, or above the Eddington Limit, might well have have large values of changing mass accretion rate,

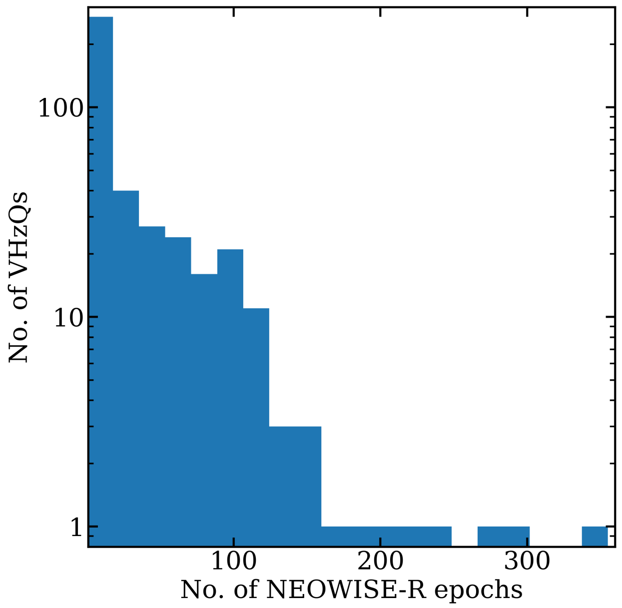


**Figure 4.** Histogram showing the number of NEOWISE-R epochs and detections there are for each VH$z$Q.

$m_{\rm accr}$. A consequence of this would be that these quasar exhibit signs of variability, most likely showing up in their UV/optical rest-frame spectra. We look for evidence of this variability signature in the NIR and MIR light-curves of the VH$z$Qs. As a guide, C IV enters the $Y$-band at redshift $z$=5.32 and exits at $z$=5.99, and enters the $J$-band at redshift $z = 6.55$ and exits at $z$=7.57. Mg II enters the $H$-band at redshift $z = 4.33$ and exits at $z = 5.37$ and enters the $K$-band at redshift $z = 6.25$ and exits at 7.50.

Using the extended datasets described in Section 2.3 and **??**, we

Figure 4 gives the number of NEOWISE-R epochs and detections there are for each VH$z$Q, while Figure **??** presents three examples of the MIR lightcurves and associated colour changes. Here we show J0100+2802 (Wu et al. 2015), J0224-4711 and J1626+2751. **NJC: What about NIR light-curves / combined light-curves**

### 3.4 Colours

Currently, very high-redshift quasars are identified by their morphology, flux and colours in optical and infrared imaging data Fan (1999); **?** Quasars are generally selected to be point sources, but be outliers from the stellar locus in colour space. For VH$z$Qs, the main technique is to look for objects with extreme optical-to-near-infrared colours The lack of proper motion can also help identified quasars (e.g. Lang et al. 2009).

Pellentesque vel elit neque, in interdum lacus. Quisque sodales, nunc et luctus convallis, nisl dui luctus dui, at congue urna velit a nisl. Ut sit amet sapien a risus dapibus sagittis. Cras sed ultricies erat. Donec id metus sed urna lacinia convallis vel sed enim. Proin nisi libero, ornare vel bibendum eu, sollicitudin sed leo. Cras tincidunt aliquet ultricies. Cras pretium velit leo, in malesuada enim. Duis sagittis ultricies interdum. Proin sit amet sem nec metus feugiat pharetra.

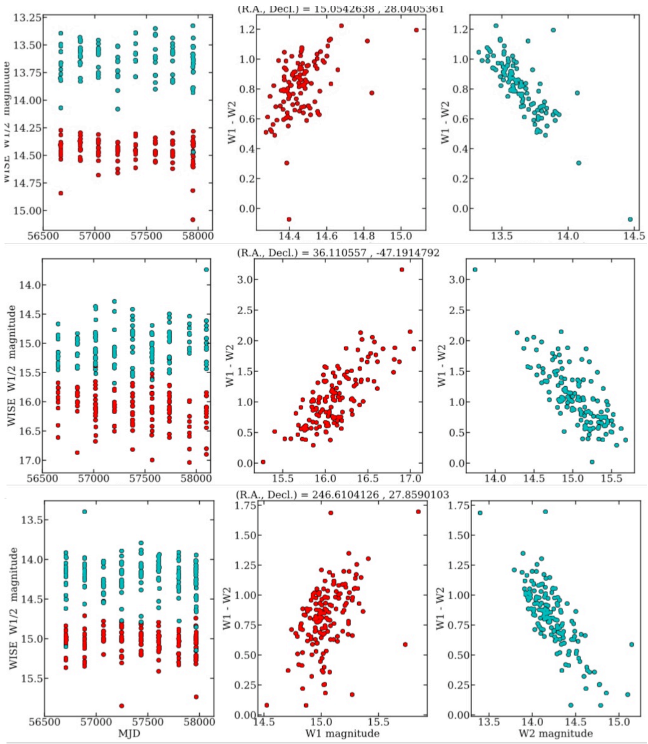


**Figure 5.** Here we show the MIR NEOWISE-R for J0100+2802 (Wu et al. 2015), J0224-4711 and J1626+2751. Red points are the W1 band; cyan points the W2 band.

Figure 6 presents the optical colour-redshift trends for Late Type M/L/T dwarfs and the VH$z$Qs.

Figure 6 presents the near-infrared colour-redshift trends for Late Type M/L/T dwarfs and the VH$z$Qs.

### 3.5 L-$z$ Plane

Having obtained an as-near-to-homogenous set of photometry as we can, we are now in a position to calculate the Absolute Magnitudes of the VH$z$Q sample and in particulare the absolute magnitude at rest-frame 1450Å' $M_{1450}$, which is a key physical quantity and goes directly towards the quasar luminosity function and thus the reionization of hydrogen calculation.

At $z = 5.00$, the rest-frame 1450Å emission is redshifted to 8700Å iobserved, i.e., in the $z$-band, while at

### 3.6 SEDs and Dust properties of the VH$z$Qs

There are a range of IR SEDs e.g. Mullaney et al. (2013) etc. etc. etc. However, they are, for our purposes all roughly the same.

## 4 DISCUSSION AND CONCLUSIONS

In this study, we have, for the first time, ompiled the list of all $z > 5$ spectroscopically confirmed quasars. We

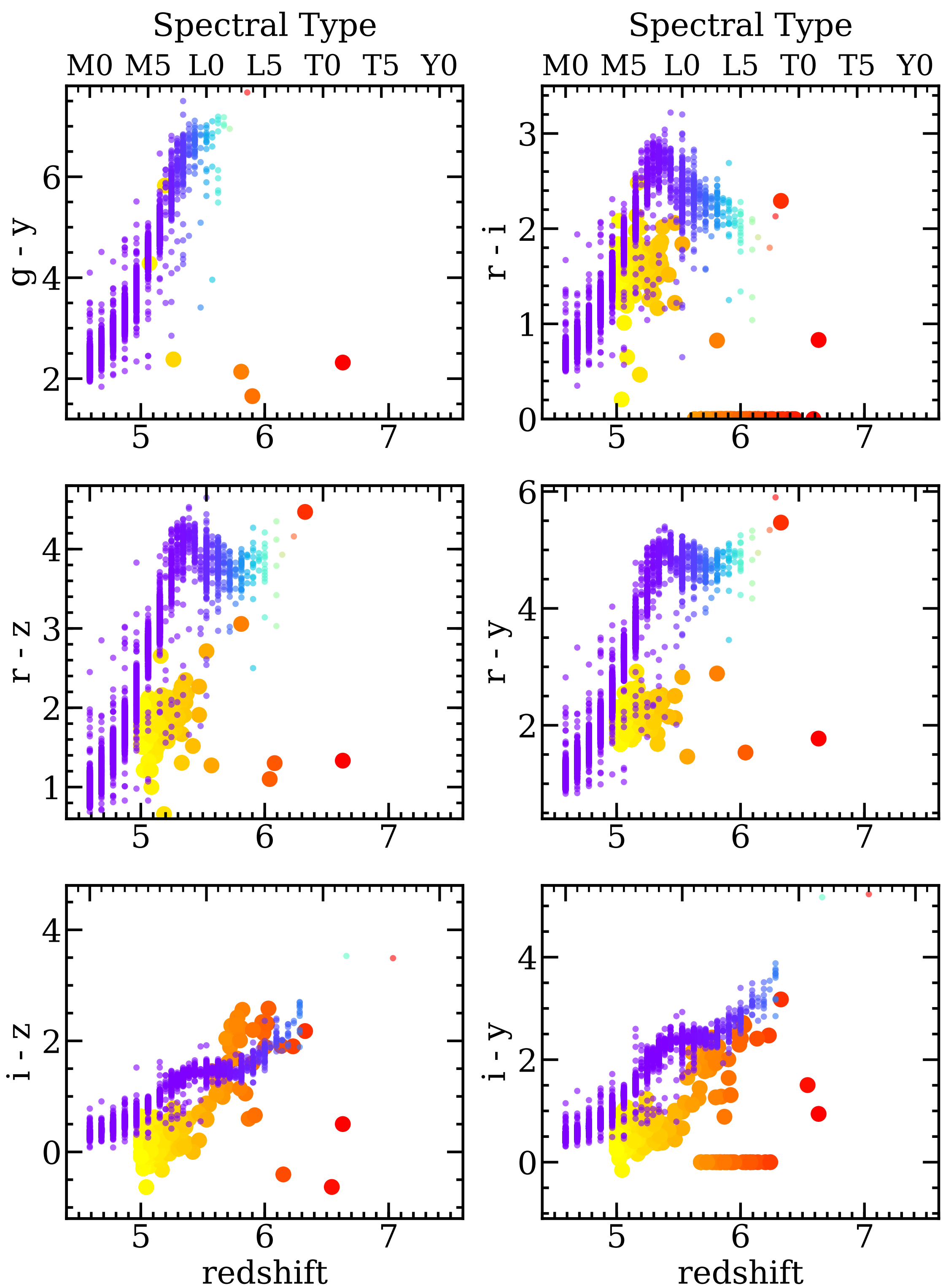




**Figure 6.** Optical colour vs. spectral type and redshift for Late Type M/L/T dwarfs and the VH$z$Qs. The stars are M, L, and T dwarfs from the Best et al. (2018) PS1-detected catalog. *N.B. Trying to look as good as Fig. 5 from Best et al. (2018). How does one get bigger gaps between subplots??*

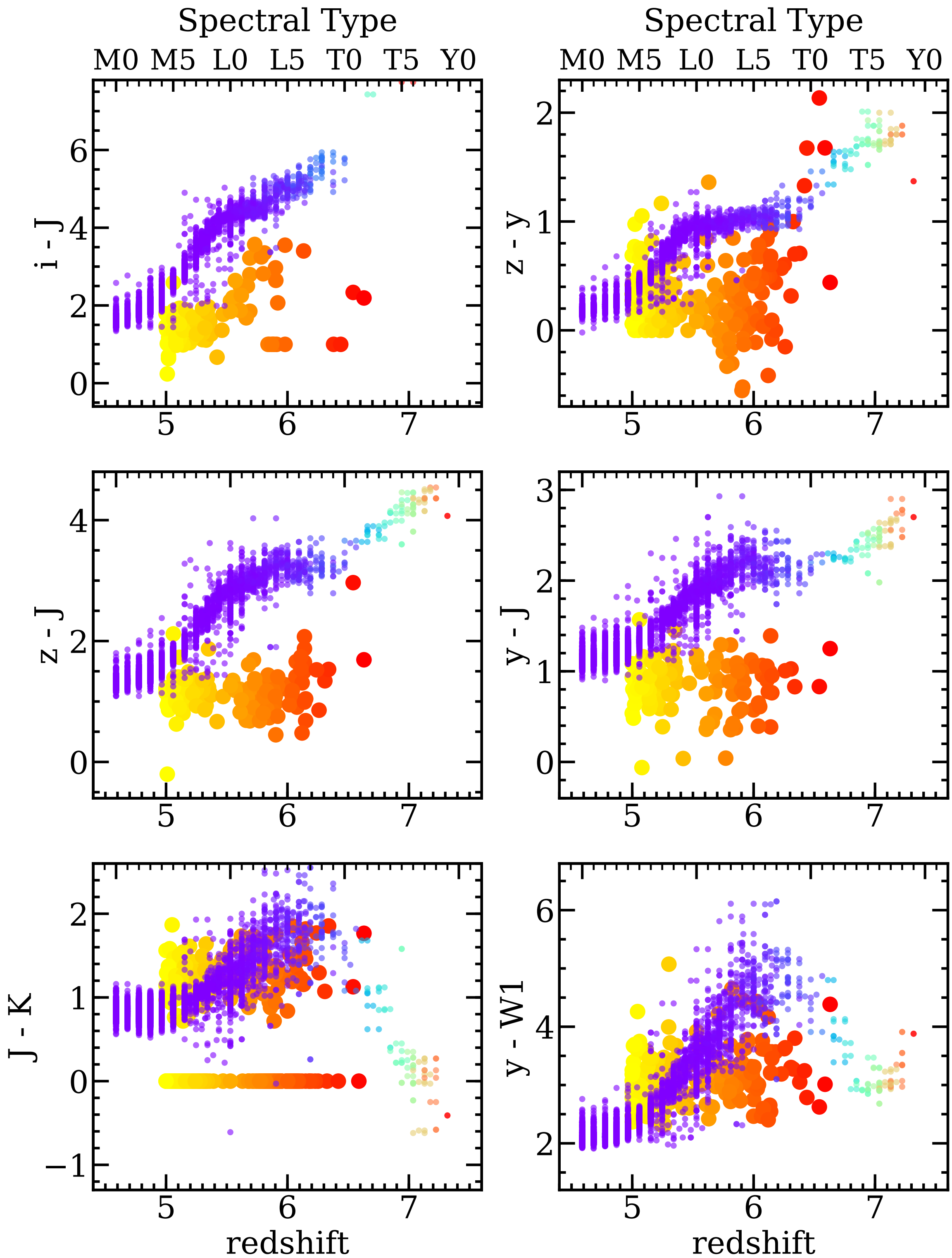


**Figure 7.** Infrared colour-spectral type and redshift plots for Late Type M/L/T dwarfs and the VH$z$Qs. *NB* I'm really not sure how Best et al. actually get their stellar sequence so clean. There are two types of spectral classification, but restricting it to just SpT_optn or SpT_nir removes the blue or red end respectively. Hmmm....

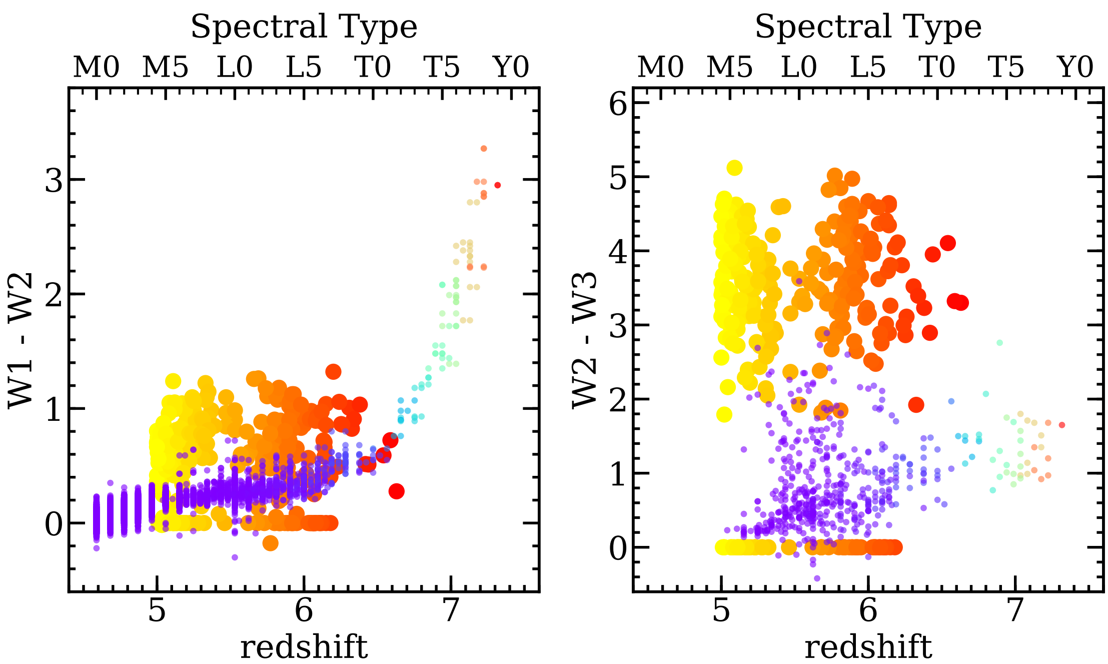


**Figure 8.** Infrared colour-spectral type and redshift plots for Late Type M/L/T dwarfs and the VH$z$Qs.

have assemble the NIR ($y/Y, J, H, K/K_s$) and MIR (WISE W1/2/3/4) photometry for these objects, given their detection rates and SEDs. We find that:

We can gain a good appreciation for what these missions will discover by collating the datasets we currently have.

- Lorem ipsum dolor sit amet, consectetur adipiscing elit. Aliquam porta sodales est, vel cursus risus porta non. Vivamus vel pretium velit. Sed fringilla suscipit felis, nec iaculis lacus convallis ac.
- Fusce pellentesque condimentum dolor, quis vehicula tortor hendrerit sed. Class aptent taciti sociosqu ad litora torquent per conubia nostra, per inceptos himenaeos. Etiam interdum tristique diam eu blandit. Donec in lacinia libero.
- Sed elit massa, eleifend non sodales a, commodo ut felis. Sed id pretium felis. Vestibulum et turpis vitae quam aliquam convallis. Sed id ligula eu nulla ultrices tempus. Phasellus mattis erat quis metus dignissim malesuada. Nulla tincidunt quam volutpat nibh facilisis euismod. Cras vel auctor neque. Nam quis diam risus.

Nunc lacus nibh, convallis ac lobortis ut, tempus ac lectus. Maecenas eu elit massa. Nulla vel lacus lorem. Proin et lobortis tortor. Phasellus ultrices nisl non enim porttitor dictum. Curabitur nec nunc ac nibh ornare elementum. Nunc ultrices hendrerit ultricies. Aliquam dapibus semper est et gravida. Etiam cursus, massa eget tempor elementum, lectus urna feugiat nisi, eget sagittis.

## Author Contributions

N.P.R. initiated the project, compiled the list of $z > 5.00$ quasars, wrote most of the analysis code, developed the the plotting scripts, and developed and wrote the initial and subsequent drafts of the manuscript.

N.J.G.C. supplied the critical near-infrared expertise and database for which the bulk of the project relies. N.J.G.C. also contributed directly to the writing of the manuscript.

## Availability of Data and computer analysis codes

All materials, data, code and analysis algorithms are fully available at: `https://github.com/d80b2t/VHzQ`

## ACKNOWLEDGEMENTS

NPR acknowledges support from the STFC and the Ernest Rutherford Fellowship scheme.

We thank Mike Read at the ROE WFAU for help with the WFCAM Science Archiv (WSA), and also the VISTA Science Archive (VSA). We thank Bernie Shiao at STScI for help with the Pan-STARRS1 DR1 CasJobs interface.

This paper heavily used TOPCAT (v4.4) (Taylor 2005, 2011). This research made use of `Astropy`, a community-developed core Python package for Astronomy (Astropy Collaboration et al. 2013; The Astropy Collaboration et al. 2018).

The Pan-STARRS1 Surveys (PS1) and the PS1 public science archive have been made possible through contributions by the Institute for Astronomy, the University of Hawaii, the Pan-STARRS Project Office, the Max-Planck Society and its participating institutes, the Max Planck Institute for Astronomy, Heidelberg and the Max Planck Institute for Extraterrestrial Physics, Garching, The Johns Hopkins University, Durham University, the University of Edinburgh, the Queen's University Belfast, the Harvard-Smithsonian Center for Astrophysics, the Las Cumbres Ob-

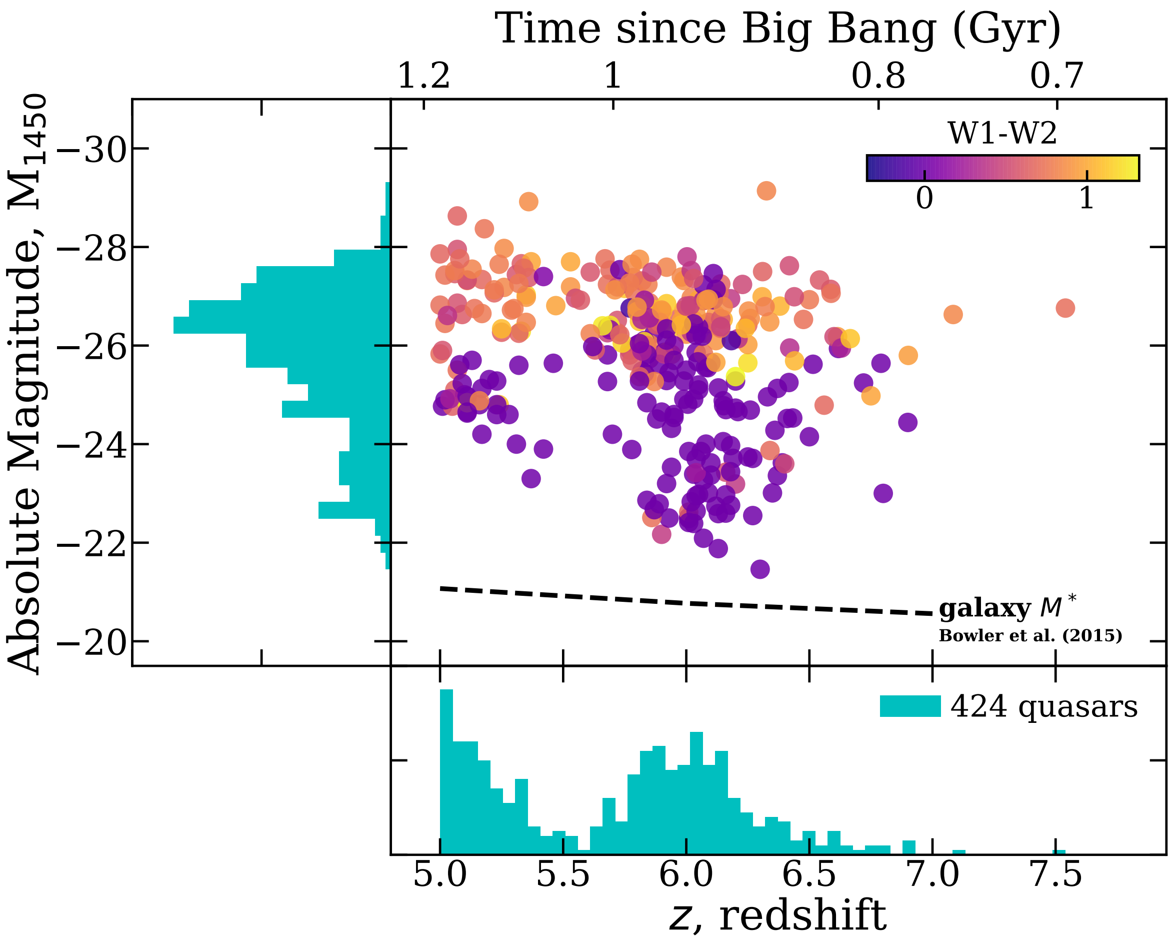


**Figure 9.** The spectral bands used by different survey telescopes and that are relevant here.

servatory Global Telescope Network Incorporated, the National Central University of Taiwan, the Space Telescope Science Institute, the National Aeronautics and Space Administration under Grant No. NNX08AR22G issued through the Planetary Science Division of the NASA Science Mission Directorate, the National Science Foundation Grant No. AST-1238877, the University of Maryland, Eotvos Lorand University (ELTE), the Los Alamos National Laboratory, and the Gordon and Betty Moore Foundation.

This project used data obtained with the Dark Energy Camera (DECam) and the NOAO Data Lab, The Data Lab is operated by the National Optical Astronomy Observatory, the national center for ground-based nighttime astronomy in the United States operated by the Association of Universities for Research in Astronomy (AURA) under cooperative agreement with the National Science Foundation.

This publication makes use of data products from the Wide-field Infrared Survey Explorer, which is a joint project of the University of California, Los Angeles, and the Jet Propulsion Laboratory/California Institute of Technology, and NEOWISE, which is a project of the Jet Propulsion Laboratory/California Institute of Technology. WISE and NEOWISE are funded by the National Aeronautics and Space Administration.

CasJobs was originally developed by the Johns Hopkins University/ Sloan Digital Sky Survey (JHU/SDSS) team. With their permission, MAST used version 3.5.16 to construct CasJobs-based tools for GALEX, Kepler, the Hubble Source Catalog, and PanSTARRS.

This research has made use of the SVO Filter Profile Service (http://svo2.cab.inta-csic.es/theory/fps/) supported from the Spanish MINECO through grant AyA2014-55216 The SVO Filter Profile Service[11] describes the Spanish VO Filter Profile Service. The Filter Profile Service Access Protocol. Rodrigo, C., Solano, E. http://ivoa.net/documents/Notes/SVOFPSDAL/index.html

[11] Rodrigo, C., Solano, E., Bayo, A. http://ivoa.net/documents/Notes/SVOFPS/index.html

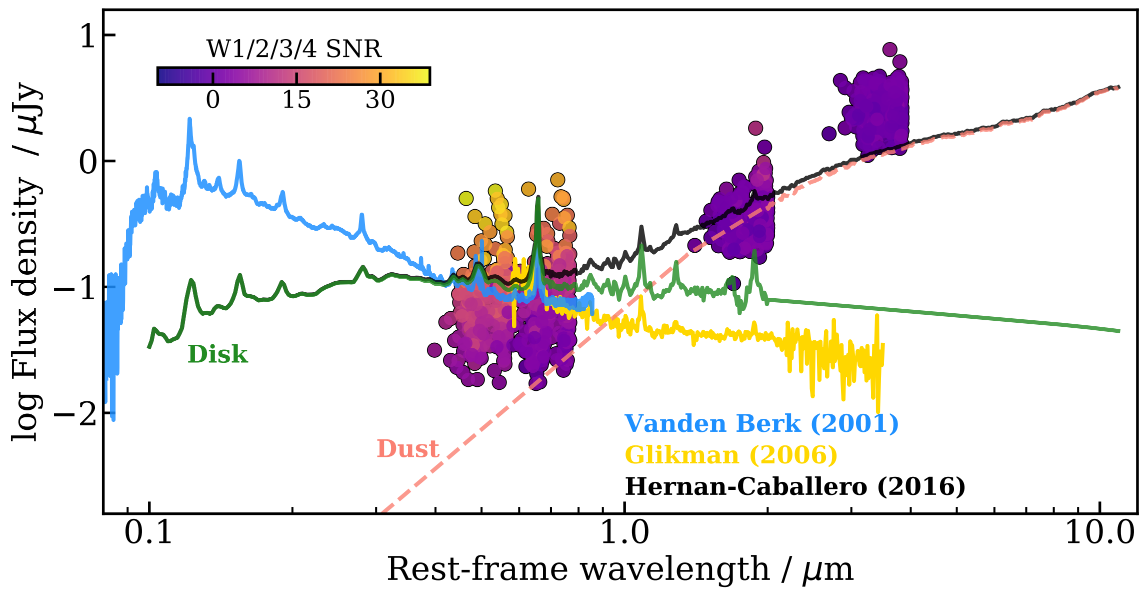


**Figure 10.** The rest-frame properties of the VH$z$Qs.

## APPENDIX A: A. PHOTOMETRIC BANDS AND CONVERSIONS

Due to the differing normalizations between the SDSS and UKIDSS photometric systems, certain corrections are required. To present our data in the purest sense, all the NIR magnitudes from UKIDSS (originally AB magnitudes) were corrected to Vega magnitudes as suggested in Hewett et al. (2006).

Although ULAS magnitudes are reported in terms of Vega and SDSS magnitudes are reported in AB terms for the most part whenever an optical-NIR color was calculated both magnitudes were left in their default term.

https://www.gemini.edu/sciops/instruments/magnitudes-and-fluxes

## APPENDIX B: NOTES ON INDIVIDUAL OBJECTS

### B1 VDES J0020-3653

VDES J0020-3653, has not, at the time of writing been published, but the redshift is public and it is in the JWST GTO target lists: JSP/JWST GTO NIRSpec Observations and phase2-public/1222.pdf.

### B2 PSO J006.1240+39.2219

Tang et al. (2017) and Koptelova et al. (2017) report PSO J006.1240+39.2219, separately but ≈contemporarily.

## APPENDIX C: SDSS J0901+161 AND PSO J135.3860+16.2518

SDSS J0901+1615 and PSO J135.3860+16.2518 are reported in **?** and Bañados et al. (2015). We use the earlier reference in 1.

## APPENDIX D: SDSS J0906+6930

BWE 910901+6942 at $z = 5.47$ in Leipski et al. (2014) and **?** we assign as SDSS J0906+6930.

### D1 J0923+0402

J0923+0402 is reported by Matsuoka et al. (2018b) from the SHELLQs and in **?** from the DELS. We note the initial report from HSC as the one presented in our 1.

## REFERENCES


Agarwal B., Smith B., Glover S., Natarajan P., Khochfar S., 2016, MNRAS, 459, 4209

Alexander T., Natarajan P., 2014, Science, 345, 1330

Ashby M. L. N., et al., 2013, ApJS, 209, 22

Assef R. J., Stern D., Noirot G., Jun H. D., Cutri R. M., Eisenhardt P. R. M., 2018, ApJS, 234, 23

Astropy Collaboration et al., 2013, Astron. & Astrophys., 558, A33

Bañados E., Decarli R., Walter F., Venemans B. P., Farina E. P., Fan X., 2015, ApJ Lett., 805, L8

Bañados E., et al., 2014, AJ, 148, 14

Bañados E., et al., 2016, ApJS, 227, 11

Bañados E., et al., 2018, Nat, 553, 473

Becker G. D., Bolton J. S., Lidz A., 2015, PASA, 32, 45

**Table A1.** Adapted from Table 9 of Peth et al. (2011). CTIO/DECam, PanSTARRS/PS1, LSST Filter only values. All wavelengths in Å. From González-Fernández et al. (2018) $Z_{\rm AB} - Z_{\rm Vega} = 0.502$; $Y_{\rm AB} - Y_{\rm Vega} = 0.600$; $J_{\rm AB} - J_{\rm Vega} = 0.916$; $H_{\rm AB} - H_{\rm Vega} = 1.366$; $Ks_{\rm AB} - Ks_{\rm Vega} = 1.827$; and the CASU Vega to AB conversions v1.3:: Z,Y,J,H,Ks were: 0.524, 0.618, 0.937, 1.384, 1.839. So, Δ(vs. Gonzalez-Fernandez):: (11.2, 1.1, 5.4, 1.6, 0.1) millimags. Δ(vsCASU v1.3):: (-10.8, -16.9, -15.6, -16.4, -11.9) millimags.

| Band | $\lambda_{\rm eff}$ | $\lambda_{\rm min}$ | $\lambda_{\rm max}$ | $W_{\rm eff}$ | AB - Vega | Transformations |
|---|---|---|---|---|---|---|
| $g_{\rm HSC}$ | 4633 | 3940 | 5546 | 1460 | $g_{\rm HSC}$ | $= g_{\rm AB} + 0.097$ |
| $g_{\rm LSST}$ | 4730 | 3877 | 5665 | 1333 | $g_{\rm LSST}$ | $= g_{\rm AB} + 0.083$ |
| $g_{\rm DECam}$ | 4734 | 3939 | 5528 | 1133 | $g_{\rm DECam}$ | $= g_{\rm AB} + 0.083$ |
| $g_{\rm PS1}$ | 4776 | 3943 | 5593 | 1167 | $g_{\rm PS1}$ | $= g_{\rm AB} + 0.080$ |
| | | | | | | |
| $r_{\rm HSC}$ | 6104 | 5325 | 7071 | 1503 | $r_{\rm HSC}$ | $= r_{\rm AB} - 0.151$ |
| $r_{\rm PS1}$ | 6130 | 5386 | 7036 | 1318 | $r_{\rm PS1}$ | $= r_{\rm AB} - 0.153$ |
| $r_{\rm LSST}$ | 6139 | 5375 | 7055 | 1338 | $r_{\rm LSST}$ | $= r_{\rm AB} - 0.155$ |
| $r_{\rm DECam}$ | 6345 | 5506 | 7238 | 1379 | $r_{\rm DECam}$ | $= r_{\rm AB} - 0.192$ |
| | | | | | | |
| $i_{\rm PS1}$ | 7485 | 6778 | 8304 | 1243 | $i_{\rm PS1}$ | $= i_{\rm AB} - 0.369$ |
| $i_{\rm LSST}$ | 7487 | 6765 | 8325 | 1209 | $i_{\rm LSST}$ | $= i_{\rm AB} - 0.369$ |
| $i_{\rm HSC}$ | 7633 | 6791 | 8658 | 1483 | $i_{\rm PS1}$ | $= i_{\rm AB} - 0.396$ |
| $i_{\rm DECam}$ | 7750 | 6950 | 8646 | 1371 | $i_{\rm DECam}$ | $= i_{\rm AB} - 0.415$ |
| | | | | | | |
| $z_{\rm PS1}$ | 8658 | 8028 | 9346 | 966 | $z_{\rm PS1}$ | $= z_{\rm AB} - 0.508$ |
| $z_{\rm LSST}$ | 8669 | 8035 | 9375 | 994 | $z_{\rm LSST}$ | $= z_{\rm AB} - 0.509$ |
| $Z_{\rm VIRCAM}$ | 8762 | 8157 | 9400 | 978 | $Z_{\rm VIRCAM}$ | $= z_{\rm AB} - 0.513$ |
| $Z_{\rm WFCAM}$ | 8802 | 8129 | 9457 | 926 | $Z_{\rm WFCAM}$ | $= z_{\rm AB} - 0.514$ |
| $z_{\rm HSC}$ | 8915 | 8280 | 9498 | 793 | $Z_{\rm HSC}$ | $= z_{\rm AB} - 0.512$ |
| $z_{\rm DECam}$ | 9216 | 8360 | 10166 | 1502 | $z_{\rm DECam}$ | $= z_{\rm AB} - 0.521$ |
| | | | | | | |
| $y_{\rm PS1}$ | 9603 | 9100 | 10838 | 615 | $y_{\rm PS1}$ | $= y_{\rm AB} - 0.541$ |
| $y_{\rm LSST}$ | 9677 | 9089 | 10859 | 810 | $y_{\rm LSST}$ | $= y_{\rm AB} - 0.546$ |
| $Y_{\rm DECam}$ | 9876 | 9355 | 10730 | 676 | $Y_{\rm DECam}$ | $= Y_{\rm AB} - 0.570$ |
| $Y_{\rm HSC}$ | 9976 | 9000 | 10931 | 1386 | $Y_{\rm HSC}$ | $= Y_{\rm AB} - 0.580$ |
| $Y_{\rm WFCAM}$ | 10305 | 9790 | 10810 | 1020 | $Y_{\rm WFCAM}$ | $= Y_{AB} - 0.617$ |
| $Y_{\rm VIRCAM}$ | 10184 | 9427 | 10977 | 905 | $Y_{\rm VISTA}$ | $= Y_{AB} - 0.601$ |
| | | | | | | |
| $J_{\rm 2MASS}$ | 12350 | 10806 | 14068 | 1624 | $J_{\rm 2MASS}$ | $= J_{AB} - 0.894$ |
| $J_{\rm VIRCAM}$ | 12464 | 11427 | 13759 | 1628 | $J_{\rm VISTA}$ | $= J_{AB} - 0.921$ |
| $J_{\rm WFCAM}$ | 12483 | 11690 | 13280 | 1590 | $J_{\rm WFCAM}$ | $= J_{AB} - 0.919$ |
| | | | | | | |
| $W_{\rm Wircam}$ | 14514 | 13890 | 15166 | 1020 | $W_{\rm Wircam}$ | $= W_{AB} - 1.163$ |
| | | | | | | |
| $H_{\rm WFCAM}$ | 16313 | 14920 | 17840 | 2920 | $H_{\rm WFCAM}$ | $= H_{AB} - 1.379$ |
| $H_{\rm VIRCAM}$ | 16310 | 14604 | 18422 | 2833 | $H_{\rm VISTA}$ | $= H_{AB} - 1.368$ |
| $H_{\rm 2MASS}$ | 16620 | 14787 | 18231 | 2509 | $H_{\rm 2MASS}$ | $= H_{AB} - 1.374$ |
| | | | | | | |
| $Ks_{\rm VIRCAM}$ | 21337 | 19333 | 23674 | 3055 | $Ks_{\rm VISTA}$ | $= Ks_{AB} - 1.83$ |
| $Ks_{\rm 2MASS}$ | 21590 | 19544 | 23552 | 2619 | $Ks_{\rm 2MASS}$ | $= Ks_{AB} - 1.84$ |
| $K_{\rm WFCAM}$ | 22010 | 20290 | 23800 | 3510 | $K_{\rm WFCAM}$ | $= K_{AB} - 1.9$ |
| | | | | | | |
| WISE W1 | 33526 | 27541 | 38724 | 6626 | W1 | $= {\rm W1_{AB}} - 2.699$ |
| WISE W2 | 46028 | 39633 | 53414 | 10423 | W2 | $= {\rm W2_{AB}} - 3.339$ |
| WISE W3 | 115608 | 74430 | 172613 | 55056 | W3 | $= {\rm W3_{AB}} - 5.174$ |
| WISE W4 | 228172 | 195201 | 279107 | 41017 | W4 | $= {\rm W4_{AB}} - 6.66$ |


Becker R. H., White R. L., Helfand D. J., 1995, ApJ, 450, 559

Best W. M. J., et al., 2018, ApJS, 234, 1

Blain A., et al., 2013, ArXiv e-prints

Bosman S. E. I., et al., 2017, MNRAS, 470, 1919

Calura F., Gilli R., Vignali C., Pozzi F., Pipino A., Matteucci F., 2014, MNRAS, 438, 2765

Carilli C. L., et al., 2007, ApJ Lett., 666, L9

Carilli C. L., et al., 2010, ApJ, 714, 834

Carnall A. C., Shanks T., Chehade B., Fumagalli M., Rauch M., Irwin M. J., Gonzalez-Solares E., Findlay J. R., Metcalfe N., 2015, MNRAS, 451, L16

Casali M., et al., 2007, Astron. & Astrophys., 467, 777

Chambers K. C., et al., 2016, arXiv:1612.05560v3

Chen S.-F. S., et al., 2017, ApJ, 850, 188

Cool R. J., et al., 2006, AJ, 132, 823

Cross N., Hambly N., Collins R., Sutorius E., Read M., Blake R., 2013, in Adamson A., Davies J., Robson I., eds, Thirty Years of Astronomical Discovery with UKIRT Vol. 37 of Astrophysics and Space Science Proceedings, Discovery of Variables in WFCAM and VISTA Data. p. 193

Cross N. J. G., Collins R. S., Mann R. G., Read M. A., Sutorius E. T. W., Blake R. P., Holliman M., Hambly N. C., Emerson

J. P., Lawrence A., Noddle K. T., 2012, Astron. & Astrophys., 548, A119
Cushing M. C., et al., 2006, ApJ, 648, 614
Cutri R. M. o., 2013, Technical report, Explanatory Supplement to the AllWISE Data Release Products
Dalton G. B., et al., 2006, in Society of Photo-Optical Instrumentation Engineers (SPIE) Conference Series Vol. 6269 of Proc. SPIE, The VISTA infrared camera. p. 62690X
De Rosa G., Decarli R., Walter F., Fan X., Jiang L., Kurk J., Pasquali A., Rix H. W., 2011, ApJ, 739, 56
Dey A., et al., 2018, ArXiv e-prints
Edge A., Sutherland W., Kuijken K., Driver S., McMahon R., Eales S., Emerson J. P., 2013, The Messenger, 154, 32
Emerson J., McPherson A., Sutherland W., 2006, The Messenger, 126, 41
Emerson J. P., Irwin M. J., Lewis J., Hodgkin S., Evans D., Bunclark P., McMahon R., Hambly N. C., Mann R. G., Bond I., Sutorius E., Read M., Williams P., Lawrence A., Stewart M., 2004, in P. J. Quinn & A. Bridger ed., Society of Photo-Optical Instrumentation Engineers (SPIE) Conference Series Vol. 5493 of Society of Photo-Optical Instrumentation Engineers (SPIE) Conference Series, VISTA data flow system: overview. pp 401–410
Fan X., 1999, AJ, 117, 2528
Fan X., Carilli C. L., Keating B., 2006, ARA&A, 44, 415
Fan X., et al., 2000, AJ, 119, 1
Fan X., et al., 2004, AJ, 128, 515
Fan X., et al., 2006, AJ, 132, 117
Fan X., Narayanan V. K., Lupton R. H., Strauss M. A., Knapp G. R., Becker R. H., White R. L., Pentericci L., et al., 2001, AJ, 122, 2833
Fan X., Strauss M. A., Schneider D. P., Becker R. H., White R. L., Haiman Z., Gregg M., Pentericci L., et al., 2003, AJ, 125, 1649
Flewelling H. A., et al., 2016, arXiv:1612.05243v2
Fukugita M., Ichikawa T., Gunn J. E., Doi M., Shimasaku K., Schneider D. P., 1996, AJ, 111, 1748
González-Fernández C., et al., 2018, MNRAS, 474, 5459
Goto T., 2006, MNRAS, 371, 769
Haardt F., Gorini V., Moschella U., Treves A., Colpi M., eds, 2016, Astrophysical Black Holes Vol. 905 of Lecture Notes in Physics, Berlin Springer Verlag
Hambly N. C., Collins R. S., Cross N. J. G., et al. 2008, MNRAS, 384, 637
Hewett P. C., Warren S. J., Leggett S. K., Hodgkin S. T., 2006, MNRAS, 367, 454
Hickox R. C., Myers A. D., Greene J. E., Hainline K. N., Zakamska N. L., DiPompeo M. A., 2017, ApJ, 849, 53
Hill A. R., Gallagher S. C., Deo R. P., Peeters E., Richards G. T., 2014, MNRAS, 438, 2317
Ikeda H., Nagao T., Matsuoka K., Kawakatu N., Kajisawa M., Akiyama M., Miyaji T., Morokuma T., 2017, ApJ, 846, 57
Jannuzi B. T., Dey A., 1999, in Weymann R., et al. eds, ASP Conf. Ser. 191: Photometric Redshifts and the Detection of High Redshift Galaxies p. 111
Jiang L., et al., 2006, AJ, 132, 2127
Jiang L., et al., 2008, AJ, 135, 1057
Jiang L., et al., 2009, AJ, 138, 305
Jiang L., et al., 2010, Nat, 464, 380
Jiang L., McGreer I. D., Fan X., Bian F., Cai Z., Clément B., Wang R., Fan Z., 2015, AJ, 149, 188
Kaiser N., et al., 2002, in J. A. Tyson & S. Wolff ed., Society of Photo-Optical Instrumentation Engineers (SPIE) Vol. 4836, Pan-STARRS: A Large Synoptic Survey Telescope Array. pp 154–164
Kaiser N., et al., 2010, in Society of Photo-Optical Instrumentation Engineers (SPIE) Vol. 7733, The Pan-STARRS wide-field optical/NIR imaging survey. p. 0
Kashikawa N., Ishizaki Y., Willott C. J., Onoue M., Im M., Furusawa H., Toshikawa J., Ishikawa S., Niino Y., Shimasaku K., Ouchi M., Hibon P., 2015, ApJ, 798, 28
Kim Y., et al., 2015, ApJ Lett., 813, L35
Koptelova E., Hwang C.-Y., Yu P.-C., Chen W.-P., Guo J.-K., 2017, Scientific Reports, 7, 41617
Kurk J. D., et al., 2007, ApJ, 669, 32
Kurk J. D., Walter F., Fan X., Jiang L., Jester S., Rix H.-W., Riechers D. A., 2009, ApJ, 702, 833
Lacy M., et al., 2004, ApJS, 154, 166
Lambrides E. L., Petric A. O., Tchernyshyov K., Zakamska N. L., Watts D. J., 2018, ArXiv e-prints
Lang D., Hogg D. W., Jester S., Rix H., 2009, AJ, 137, 4400
Latif M. A., Volonteri M., Wise J. H., 2018, arXiv:1801.07685v1
Lawrence A., et al., 2007, MNRAS, 379, 1599
Le Fèvre O., et al., 2003, in Iye M., Moorwood A. F. M., eds, Instrument Design and Performance for Optical/Infrared Ground-based Telescopes Vol. 4841 of Proc. SPIE, Commissioning and performances of the VLT-VIMOS instrument. pp 1670–1681
Leipski C., et al., 2014, ApJ, 785, 154
Lupi A., Haardt F., Dotti M., Fiacconi D., Mayer L., Madau P., 2016, MNRAS, 456, 2993
Madau P., Haardt F., Dotti M., 2014, ApJ Lett., 784, L38
Magnier E. A., et al., 2016a, arXiv:1612.05242v2
Magnier E. A., et al., 2016b, arXiv:1612.05244v2
Magnier E. A., et al., 2016c, arXiv:1612.05240v2
Mahabal A., Stern D., Bogosavljević M., Djorgovski S. G., Thompson D., 2005, ApJ Lett., 634, L9
Mainzer A., et al., 2011, ApJ, 731, 53
Mainzer A., et al., 2014, ApJ, 792, 30
Matsuoka Y., et al., 2016, ApJ, 828, 26
Matsuoka Y., et al., 2018a, PASJ, 70, S35
Matsuoka Y., et al., 2018b, ApJS, 237, 5
Mazzucchelli C., et al., 2017, ApJ, 849, 91
McGreer I. D., Becker R. H., Helfand D. J., White R. L., 2006, ApJ, 652, 157
McGreer I. D., et al., 2013, ApJ, 768, 105
Miyazaki S., et al., 2018, PASJ, 70, S1
Morganson E., et al., 2012, AJ, 143, 142
Mortlock D., 2016, in Mesinger A., ed., Understanding the Epoch of Cosmic Reionization: Challenges and Progress Vol. 423 of Astrophysics and Space Science Library, Quasars as Probes of Cosmological Reionization. p. 187
Mortlock D. J., et al., 2009, Astron. & Astrophys., 505, 97
Mortlock D. J., et al., 2011, Nat, 474, 616
Mullaney J. R., Alexander D. M., Fine S., Goulding A. D., Harrison C. M., Hickox R. C., 2013, MNRAS, 433, 622
Oke J. B., Gunn J. E., 1983, ApJ, 266, 713
Papovich C., et al., 2016, ApJS, 224, 28
Peth M. A., Ross N. P., Schneider D. P., 2011, AJ, 141, 105
Pezzulli E., Valiante R., Schneider R., 2016, MNRAS, 458, 3047
Pezzulli E., Volonteri M., Schneider R., Valiante R., 2017, MNRAS, 471, 589
Reed S. L., et al., 2015, MNRAS, 454, 3952
Reed S. L., et al., 2017, MNRAS, 468, 4702
Rees M. J., 1984, ARA&A, 22, 471
Richards G. T., et al., 2006, ApJS, 166, 470
Sawicki M., 2002, AJ, 124, 3050
Schlafly E. F., Meisner A. M., 2018, ApJS
Shanks T., et al., 2015, MNRAS, 451, 4238
Simcoe R. A., Sullivan P. W., Cooksey K. L., Kao M. M., Matejek M. S., Burgasser A. J., 2012, Nat, 492, 79
Stern D., et al., 2005, ApJ, 631, 163
Stern D., et al., 2007, ApJ, 663, 677
Stoughton C., et al., 2002, AJ, 123, 485
Takeo E., Inayoshi K., Ohsuga K., Takahashi H. R., Mineshige S., 2018, MNRAS, 476, 673

Tang J.-J., et al., 2017, MNRAS, 466, 4568
Taylor M., , 2011, TOPCAT: Tool for OPerations on Catalogues And Tables, Astrophysics Source Code Library
Taylor M. B., 2005, in Shopbell P., Britton M., Ebert R., eds, Astronomical Data Analysis Software and Systems XIV Vol. 347 of Astronomical Society of the Pacific Conference Series, TOPCAT & STIL: Starlink Table/VOTable Processing Software. p. 29
The Astropy Collaboration et al., 2018, ArXiv e-prints
Tielens A. G. G. M., 2008, ARA&A, 46, 289
Timlin J. D., Ross N. P., et al., 2016, ApJS, 225, 1
Väisänen P., Tollestrup E. V., Willner S. P., Cohen M., 2000, ApJ, 540, 593
Valiante R., Schneider R., Graziani L., Zappacosta L., 2018, MNRAS, 474, 3825
Vanden Berk D. E., et al., 2001, AJ, 122, 549
Venemans B. P., et al., 2012, ApJ Lett., 751, L25
Venemans B. P., et al., 2013, ApJ, 779, 24
Venemans B. P., et al., 2015a, MNRAS, 453, 2259
Venemans B. P., et al., 2015b, ApJ Lett., 801, L11
Venemans B. P., McMahon R. G., Warren S. J., Gonzalez-Solares E. A., Hewett P. C., Mortlock D. J., Dye S., Sharp R. G., 2007, MNRAS, 376, L76
Venemans B. P., Walter F., Zschaechner L., Decarli R., De Rosa G., Findlay J. R., McMahon R. G., Sutherland W. J., 2016, ApJ, 816, 37
Volonteri M., 2010, A&ARv, 18, 279
Volonteri M., Silk J., Dubus G., 2015, ApJ, 804, 148
Wang F., et al., 2016, ApJ, 819, 24
Wang F., et al., 2017, ApJ, 839, 27
Wang R., et al., 2008, ApJ, 687, 848
Wang R., et al., 2011, ApJ Lett., 739, L34
Waters C. Z., et al., 2016, arXiv:1612.05245v4
Willott C. J., Albert L., Arzoumanian D., Bergeron J., Crampton D., Delorme P., Hutchings J. B., Omont A., Reylé C., Schade D., 2010, AJ, 140, 546
Willott C. J., Bergeron J., Omont A., 2015, ApJ, 801, 123
Willott C. J., et al., 2007, AJ, 134, 2435
Willott C. J., et al., 2009, AJ, 137, 3541
Willott C. J., et al., 2010, AJ, 139, 906
Willott C. J., Omont A., Bergeron J., 2013, ApJ, 770, 13
Wright E. L., Eisenhardt P. E., Fazio G. G., 1994, ArXiv Astrophysics e-prints
Wright E. L., et al., 2010, AJ, 140, 1868
Wu X.-B., et al., 2015, Nat, 518, 512
Wyithe J. S. B., Loeb A., 2003, ApJ, 586, 693
Yan L., Sajina A., Fadda D., Choi P., Armus L., Helou G., Teplitz H., Frayer D., Surace J., 2007, ApJ, 658, 778
Zeimann G. R., White R. L., Becker R. H., Hodge J. A., Stanford S. A., Richards G. T., 2011, ApJ, 736, 57